**H1prelim-08-073** Submitted to

**XVI International Workshop on Deep-Inelastic Scattering, DIS2008**, April 7-11, 2008, London
Parallel Session **Heavy Flavours**

*Electronic Access:https://www-h1.desy.de/publications/H1preliminary.short_list.html*

# Measurement of $\mathrm{D}^{*}$ Meson Production in Photoproduction

H1 Collaboration

**Abstract**

Inclusive production of $D^{*}$ mesons in Photoproduction at HERA is presented. The data was collected with the H1 detector in the end of the year 2006 and in 2007 and corresponds to an integrated luminosity of 93 pb$^{-1}$. This analysis covers a kinematic region of small photon virtuality $Q^2 < 2\,\mathrm{GeV}^2$ and photon-proton center-of-mass energies of $100 < W_{\gamma p} < 285\,\mathrm{GeV}$. The $D^{*}$ meson is measured for $p_t(D^{\star}) > 1.8$ GeV and $|\eta(D^{\star})| < 1.5$. Single and double differential cross sections are compared to the NLO calculation FMNR and the LO MC programs PHYTHIA and Cascade.

# 1 Results of the Measurement

## 1.1 D* - Signal

The charm quark is tagged by a $D^*$ meson which decays in the golden channel $D^{\star\pm} \rightarrow D^0\pi^\pm_{\text{slow}} \rightarrow K^\mp\pi^\pm\pi^\pm_{\text{slow}}$. The slow pion is created just above its mass threshold and therefore its transverse momentum $p_t$ is small. In order to calculate the total $D^*$ meson production cross section the branching ratio from the PDG, $2.59\%$, is used. The number of $D^*$ mesons is extracted from the distribution of the mass difference $\Delta M$, determined as:

$$\Delta M = M(K\pi\pi_{\text{slow}}) - M(K\pi)\ . \tag{1}$$

Applying the complete event selection for Photoproduction and for $D^*$ meson candidates one gets the $\Delta M$-distribution shown in figure 1.
Table 1 shows the definition of the visible range for which the measured cross sections are quoted. Table 2 summarizes the selection cuts for which the data are corrected by the selection efficiency determined from the Monte Carlo simulation.

| Name | Range |
|---|---|
| $p_t(D^\star)$ | $>$ 1.8 GeV |
| $\lvert\eta(D^\star)\rvert$ | $<$ 1.5 |
| Virtuality | $Q^2 < 2$ GeV$^2$ |
| Inelasticity | $0.1 < y < 0.8$ |

Table 1: Definition of the visible range of the measurement.

| Name | Range |
|---|---|
| $p_t(D^\star)$ | $>$ 1.8 GeV |
| $\lvert\eta(D^\star)\rvert$ | $<$ 1.5 |
| $p_t(K)$ | $>$ 0.5 GeV |
| $p_t(\pi)$ | $>$ 0.3 GeV |
| $p_t(\pi_{\text{slow}})$ | $>$ 0.120 GeV |
| $p_t(K) + p_t(\pi)$ | $>$ 2.2 GeV |
| $\lvert M(K\pi) - M(D^0)\rvert$ | $<$ 0.08 GeV |
| $f = p_t(D^\star)/\sum_{\theta>10^\circ} E_i \cdot \sin\theta_i$ | $>$ 0.13 |

Table 2: Selection cuts for decay particles of the $D^*$ mesons. The cut on the variable f is used to supress combinatorical background. The measured cross sections are corrected for the efficiency of the selection cuts.

## 1.2 Cross-Section determination

For a cross section determination the number of $D^*$ mesons $N_{D^\star}$ and the acceptance $\text{A}_{\text{Detector}}$ and efficiency $\epsilon_{\text{Detector}}$, the trigger efficiency $\epsilon_{\text{Trigger}}$ and luminosity $\mathcal{L}$ have to be determined. The

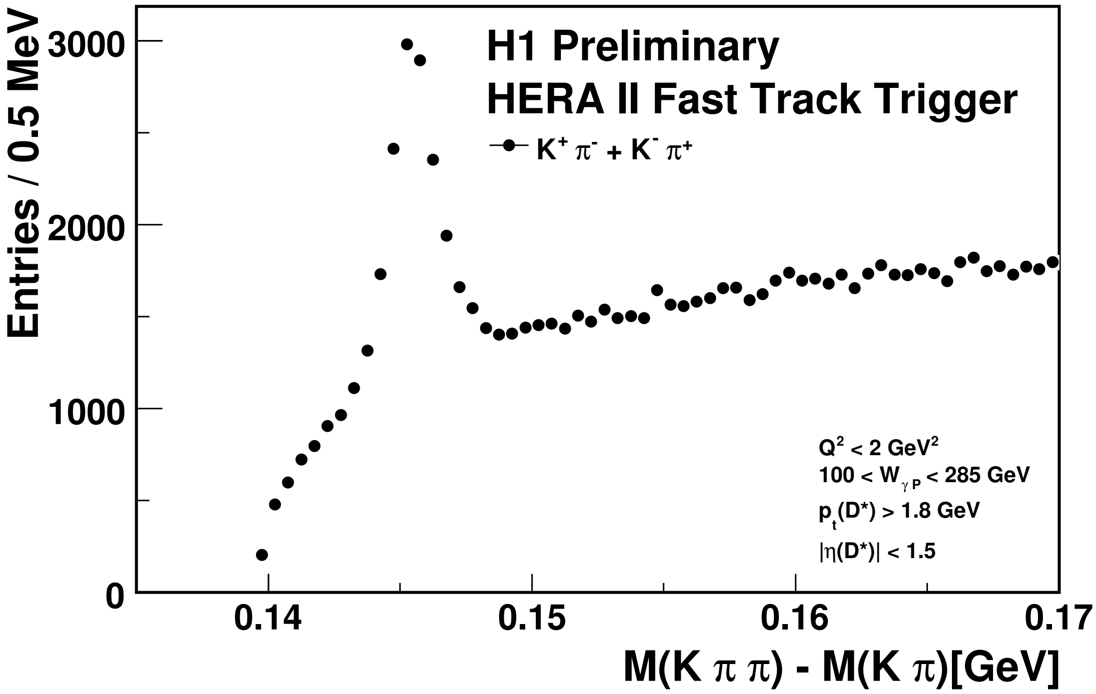


Figure 1: Distribution of the $\Delta M$ of all $D^*$ meson candidates.

bin-averaged differential cross-section $d\sigma^{\text{vis}}/dY$ for a variable $Y$ (with a bin width $\Delta Y$) is then given by the following formula:

$$\frac{d\sigma^{\text{vis}}}{dY} = \frac{N_{D^\star}(1-r)}{\Delta Y \mathcal{L} \cdot \mathcal{B}(D^\star \to K\pi\pi_{\text{slow}}) \cdot \mathrm{A}_{\text{Detector}} \cdot \epsilon_{\text{Detector}} \cdot \epsilon_{\text{Trigger}}} \,. \quad (2)$$

The correction $r = 0.04$ is applied to account for reflections from other $D^0$ decays within the $D^0$ mass window as determined in the analysis of $D^*$ production at low $Q^2$ (H1prelim-08-072) in a very similar visible range of the $D^*$ meson.

### 1.3 Results

Single- and double differential cross sections are presented in this draft. The single differential cross-sections are given for the variables $p_t(D^*)$, $\eta(D^*)$ and $W_{\gamma p}$. The double differential cross sections are given for $\eta(D^*)$ in three different $p_t(D^*)$ ranges.

The cross sections are compared to various LO Monta Carlo models as implemented in Pythia6.2 and Cascade1.2 and a NLO calculation (FMNR). The main difference between Pythia6.2 and Cascade1.2 is the treatment of the proton structure. Pythia6.2 is based on the DGLAP evolution equations whereas Cascade1.2 is based on the CCFM evolution equations. In Pythia two possibilities for the treatment of the charm-quark masses are given. The charm-quark can be treated as a massless particle or as a massive particle. In the latter case only the charm quark for the direct contribution to the cross section is caclulated massive whereas the mass of the charm quark for the resolved contribution is set to zero.

- FMNR The fixed flavour number scheme (FFNS) NLO-calculation is based on the collinear approach. The charm quarks are treated as massive partons. The fragmentation of the $D^*$ meson is done by using the peterson fragmentation function. The calculation is performed by the program FMNR.

- GMVFNS The general mass variable flavour number scheme (GMVFNS) combines the massless with the massive approach. The initial and final state facorisation scales are varied seperatley in the uncertainty determination.

The single differential cross section measurement and the comparison to LO-MC-models for $p_t(D^*)$, $\eta(D^*)$ and $W_{\gamma p}$ is shown in figures 2, 3 and 4, the comparison to the NLO calculation given by the FMNR is shown in the figures 5, 6 and 7. Double differential cross sections are presented in figures 8 and 9.

The cross section measurement, black points, is compared to different Monte-Carlo Models, represented by the different colored lines. The green histogram shows the prediction of the MC-Program Pythia6.2 where the charm-quarks are treated as massive particles, whereas the blue histogram shows the prediction by Pythia6.2 where the charm-quarks are treated as massless-particles. The red histogram shows the prediction of the MC-Program Cascade1.2.
To compare the shapes of the of the different distributions the ratio $R$ is shown in the lower part of these plots. The ratio $R$ is defined as

$$R = \frac{\frac{1}{\sigma_{vis}^{MC}} \cdot \frac{d\sigma^{MC}}{dY}}{\frac{1}{\sigma_{vis}^{data}} \cdot \frac{d\sigma^{data}}{dY}} \tag{3}$$

where $Y$ denotes the measured variable.

The Cascade prediction describes the shape of the $p_t(D^*)$ distribution (fig. 2), but is too low in normalisation. Both Pythia models are too steep. The $\eta(D^*)$ distribution (fig. 3) is described in shape and normalisation by the massless Pythia prediction, while Cascade and the massive treatment in Pythia predict a too strong decrease in the forward direction, as was already seen in the analysis of HERA I data (DESY-06-110, in a different kinematic range). The double differential measurement in $p_t(D^*)$ and $\eta(D^*)$, fig. 8, shows that all Monte Carlo programs have difficulties to describe the forward region $\eta > 0$ at large transverse momenta. In the $W_{\gamma p}$ distribution, all MC predicitions have a tendency to fall more steeply than the data.

The comparison to the NLO calculation given by the FMNR is shown in the figures 5, 6, 7, and 9. The theroretical uncertainty is estimated by an independently variation of the scales $\mu_f$, $\mu_r$ and the charm mass $m_c$. In general, the FMNR calculation gives a reasonable description of the data, but is also lower than the data in the forward direction. As for the LO MC predictions, the deficit is most prominent at large transverse momenta.

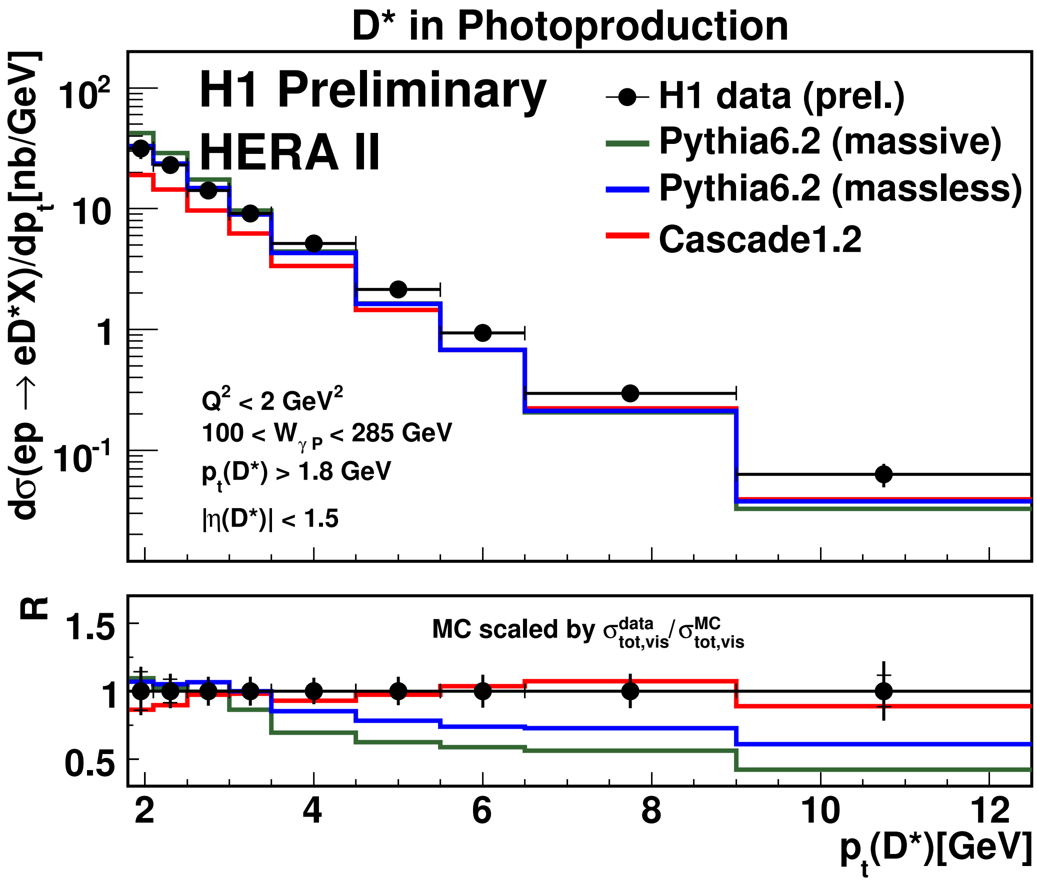


Figure 2: Differential cross section as a function of $p_t(D^*)$. The result is compared to different LO-MC models. The data are given by the black points. The green histogram shows the prediction of the MC-Program Pythia6.2 where the charm-quarks are treated as massive particles, whereas the blue histogram shows the prediction by Pythia6.2 where the charm-quarks are treated as massless-particles (for further explanations see text). The red histogram shows the prediction of the MC-Program Cascade1.2.

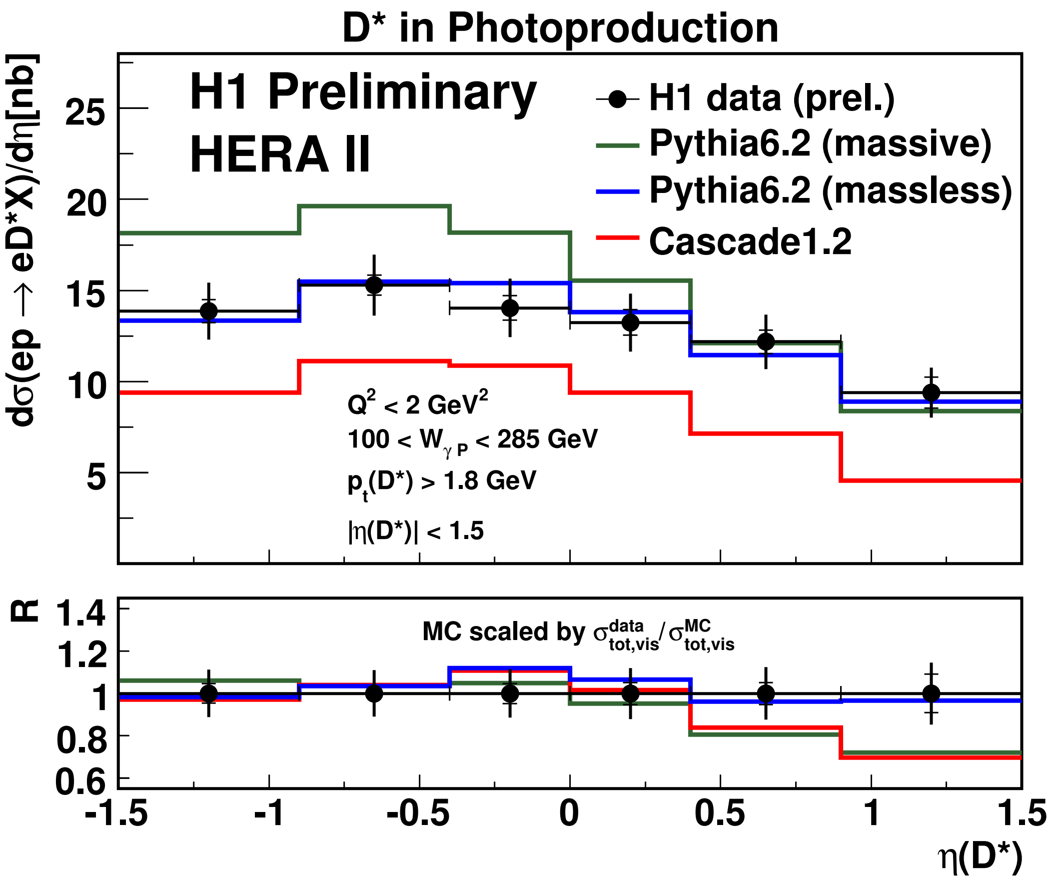


Figure 3: Differential cross section as a function of $\eta(D^*)$. The result is compared to LO-MC models. The data are given by the black points. The green histogram shows the prediction of the MC-Program Pythia6.2 where the charm-quarks are treated as massive particles, whereas the blue histogram shows the prediction by Pythia6.2 where the charm-quarks are treated as massless-particles (for further explanations see text). The red histogram shows the prediction of the MC-Program Cascade1.2.

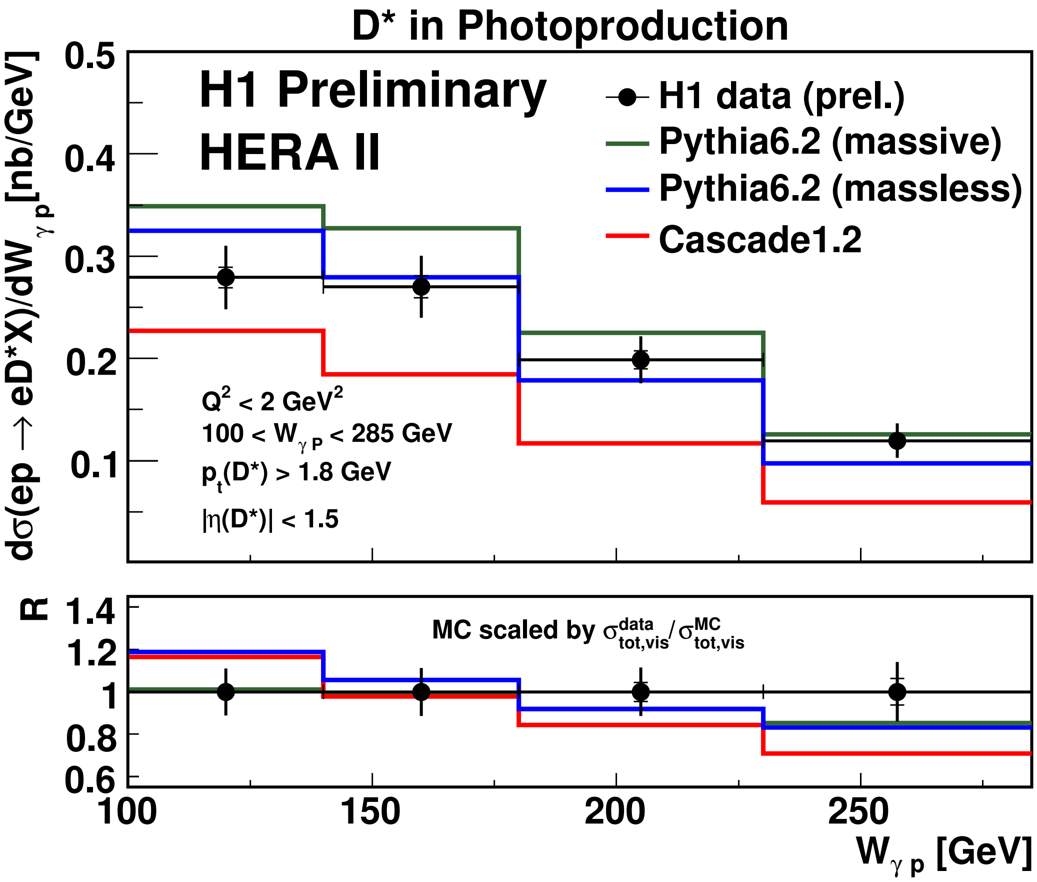


Figure 4: Differential cross section as a function of $W_{\gamma p}$. The result is compared to LO-MC models. The data are given by the black points. The green histogram shows the prediction of the MC-Program Pythia6.2 where the charm-quarks are treated as massive particles, whereas the blue histogram shows the prediction by Pythia6.2 where the charm-quarks are treated as massless-particles (for further explanations see text). The red histogram shows the prediction of the MC-Program Cascade1.2.

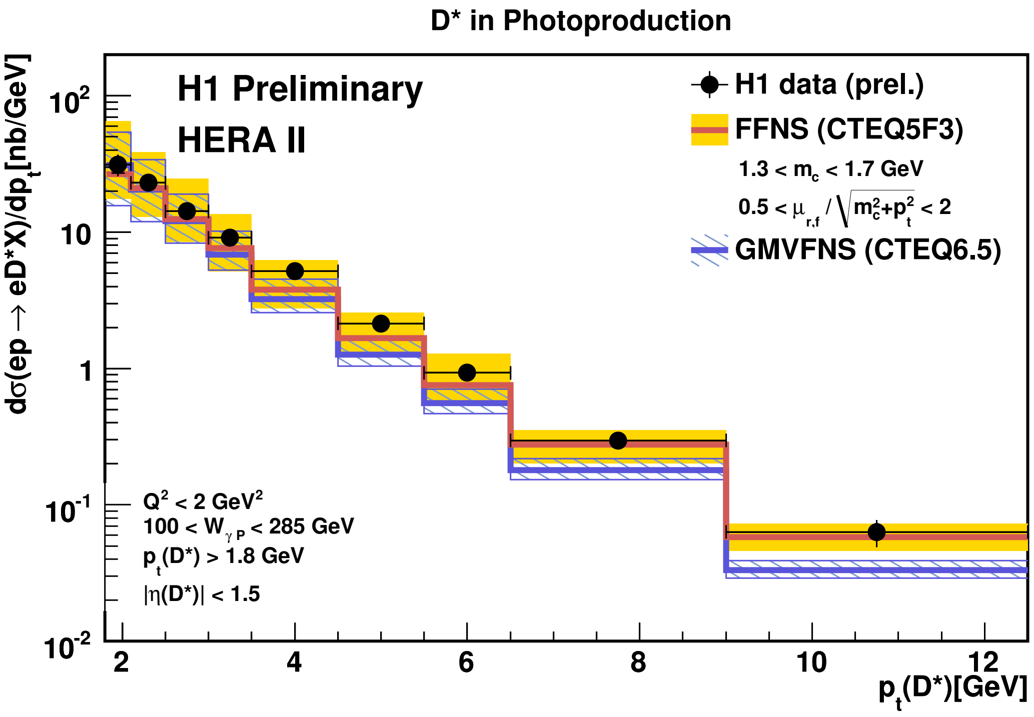


Figure 5: Differential cross section as a function of $p_t(D^*)$. The result is compared to a FFNS and GMVFNS NLO calculation.

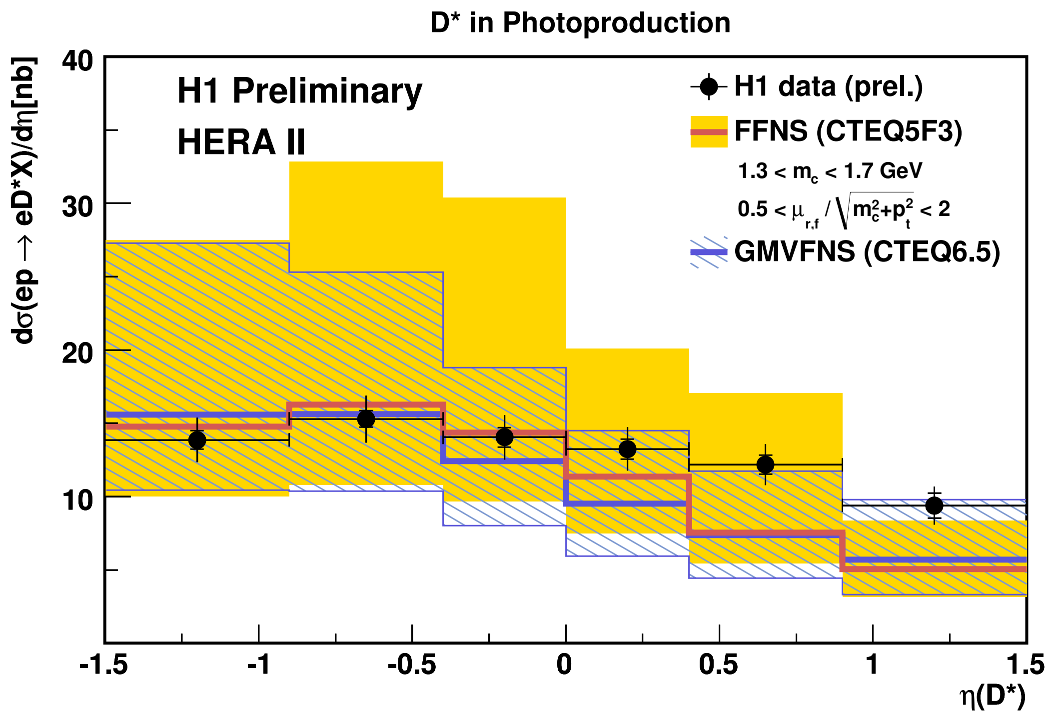


Figure 6: Differential cross section as a function of $\eta(D^*)$. The result is compared to a FFNS and GMVFNS NLO calculation.

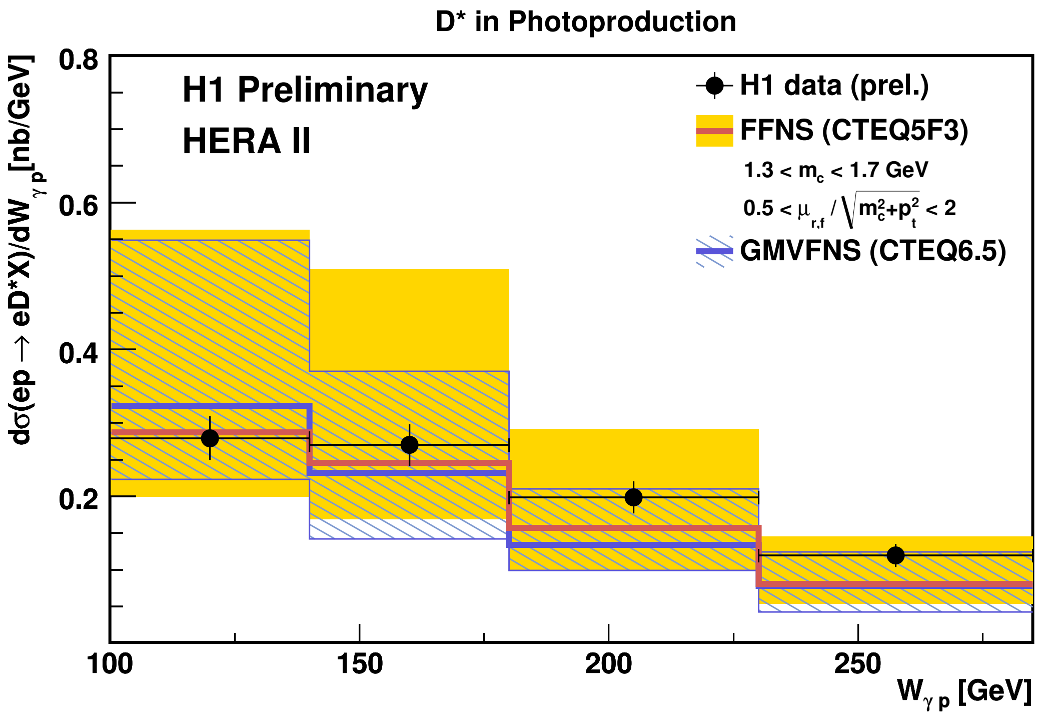


Figure 7: Differential cross section as a function of $W_{\gamma p}$. The result is compared to a FFNS and GMVFNS NLO calculation.

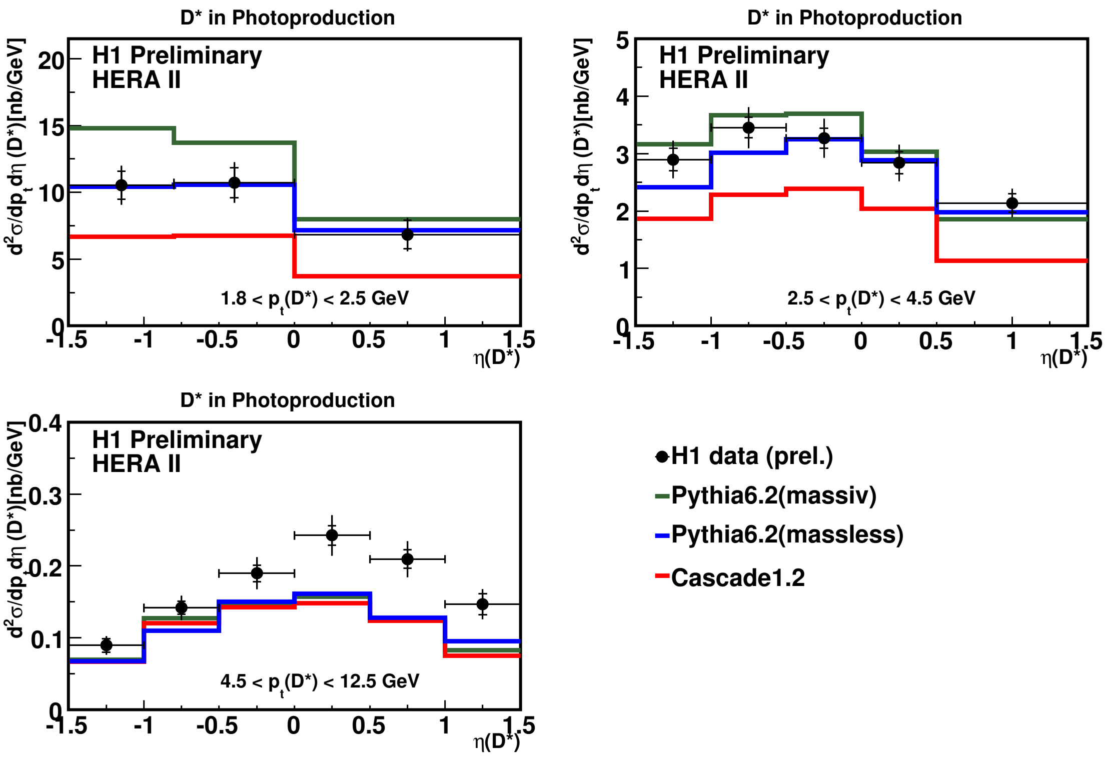


Figure 8: Double differential cross section as a function of $\eta(D^*)$ for three bins of $p_t(D^*)$. The result is compared to LO-MC models. The data are given by the black points. The green histogram shows the prediction of the MC-Program Pythia6.2 where the charm-quarks are treated as massive particles, whereas the blue histogram shows the prediction by Pythia6.2 where the charm-quarks are treated as massless-particles. The red histogram shows the prediction of the MC-Program Cascade1.2.

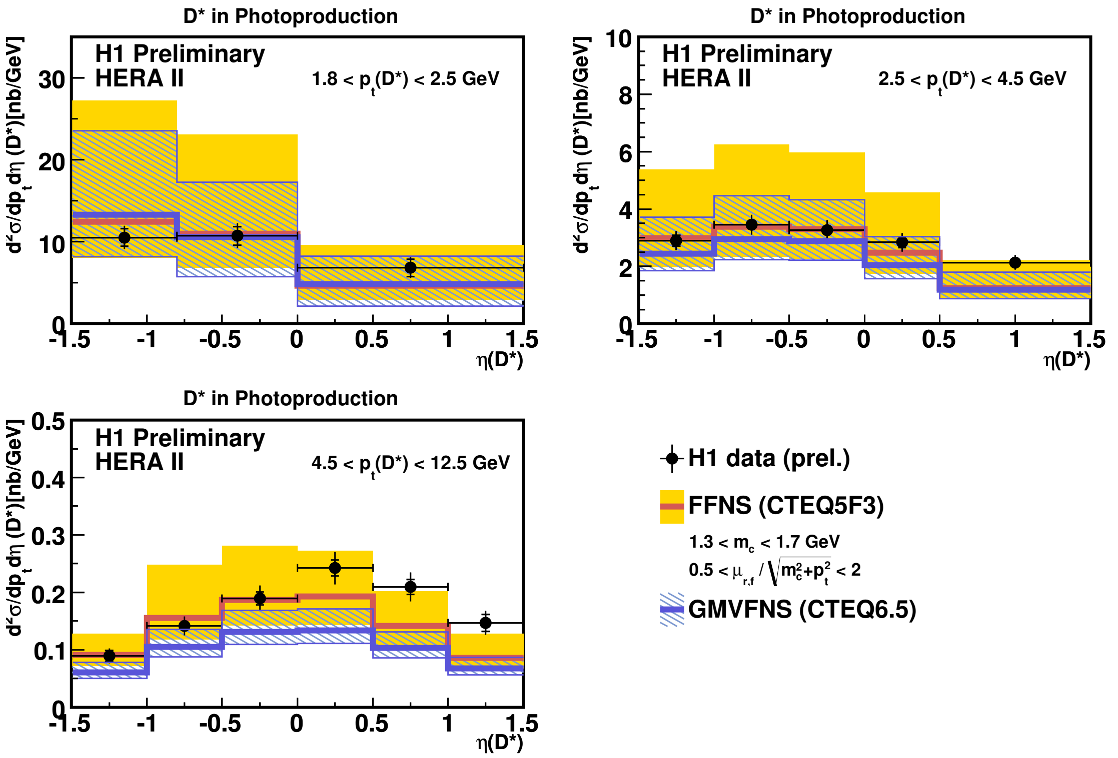


Figure 9: Double differential cross section as a function of $\eta(D^*)$ for three bins of $p_t(D^*)$. The result is compared to a FFNS and GMVFNS NLO calculation.